CrossMark

BASIC SCIENCE

Morphologic changes in the retina after selective retina therapy

Ji Ho Yang[1] · Seung-Young Yu[1] · Tae Gi Kim[1] · Eung Suk Kim[2] · Hyung Woo Kwak[1]

Abstract

Purpose To investigate structural changes in the retina by histologic evaluation and in vivo spectral domain optical coherence tomography (SD-OCT) following selective retina therapy (SRT) controlled by optical feedback techniques (OFT).

Methods SRT was applied to 12 eyes of Dutch Belted rabbits. Retinal changes were assessed based on fundus photography, fluorescein angiography (FAG), SD-OCT, light microscopy, transmission electron microscopy (TEM), and scanning electron microscopy (SEM) at each of the following time points: 1 h, and 1, 3, 7, 14 and 28 days after SRT. BrdU (5'-bromo-2'-deoxy-uridine) incorporation assay was also conducted to evaluate potential proliferation of RPE cells.

Results SRT lesions at 1 h after SRT were ophthalmoscopically invisible. FAG showed leakage in areas corresponding to SRT lesions, and hyperfluorescence disappeared after 7 days. SD-OCT showed that decreased reflectivity corresponding to RPE damage was restored to normal over time in SRT lesions. Histologic analysis revealed that the damage in SRT lesions was primarily limited to the retinal pigment epithelium (RPE) and the outer segments of the photoreceptors. SEM and TEM showed RPE cell migration by day 3 after SRT, and restoration of the RPE monolayer with microvilli by 1 week after SRT. At 14 and 28 days, ultrastructures of the RPE, including the microvilli and tight junctions, were completely restored. The outer segments of the photoreceptors also recovered without sequelae. Interdigitation between the RPE and photoreceptors was observed. BrdU incorporation assay revealed proliferation of RPE on day 3 after SRT, and peak proliferation was observed on day 7 after SRT.

Conclusion Based on multimodal imaging and histologic assessment, our findings demonstrate that SRT with OFT could selectively target the RPE without damaging the neurosensory retina. Therefore, the use of SRT with OFT opens the door to the possibility of clinical trials of well-defined invisible and nondestructive retina therapy, especially for macular disease.

Keywords Selective retina therapy (SRT) · Optical feedback technique (OFT) · Retinal pigment epithelium (RPE) · Neurosensory retina

Ji Ho Yang and Seung-Young Yu contributed equally to this work.

✉ Hyung Woo Kwak
  hwkwak@khu.ac.kr

1 Department of Ophthalmology, Kyung Hee University Hospital, Kyung Hee University, 23, Kyungheedae-ro, Dongdaemun-gu, Seoul, Republic of Korea

2 Department of Ophthalmology, Eulji University College of Medicine, Daejeon, Republic of Korea

Introduction

Retinal photocoagulation is one of the most well-established laser applications in medicine, and it is routinely performed in ophthalmic clinics worldwide to treat various retinal diseases. In conventional retinal laser photocoagulation for diabetic retinopathy, retinal vascular application is typically performed with a pulse duration of 100 to 200 ms, a laser spot diameter of 100 to 500 μm, and power of 100 to 750 mW [1]. Because of the high number of melanosomes in the RPE, it absorbs 50 to 60 % of the incident light, which is converted to heat [2]. During typical coagulation, thermal heat diffuses into the adjacent neurosensory retina, leading to the formation of ophthalmoscopically visible grayish-whitish lesions. Histologically irreversible destruction of the inner and outer segments of the photoreceptors results from strong and

extended denaturation caused by heat diffusion [3–7], and ultimately leads to irreversible laser scotoma [5, 8, 9]. In many diseases involving the macula, such as diabetic macular edema and central serous chorioretinopathy, laser scotoma develops on the macula after conventional laser therapy and may enlarge over time to spread into the area surrounding the macula [6]. Such laser scotomas can lead to severe visual loss. Macular disease is thought to be associated with dysfunction of the retinal pigment epithelium (RPE) [10], which suggests that RPE-specific treatment could improve the course of the condition by creating a new RPE barrier and improving RPE metabolism, while avoiding photoreceptor destruction [11–13].

The selective effect of laser therapy on RPE cells was first demonstrated by Roider in rabbit eyes, using 5-μs argon laser pulses at 514 nm with a 500-Hz repetition rate [14]. Roider's study demonstrated that microsecond pulses produced intracellular microbubbles around the melanosomes, which led to selective damage of RPE cells [10]. Therefore, selective laser treatment of the RPE without damage to the neural retina was termed 'selective retina therapy' (SRT). The clinical efficacy of SRT has been demonstrated for central serous chorioretinopathy, diabetic maculopathy, and macular edema secondary to branch retinal vein occlusion [12, 15–17]. Selective targeting of the RPE with SRT has also been demonstrated in a rabbit model [18]. Despite the good outcome, however, SRT laser treatment has certain limitations. Because the lesion is invisible following SRT irradiation, the laser setting must be changed for each irradiation session to confirm the appropriate laser dose. The fact that the melanin concentration varies even within the same retina further complicates the issue [19]. Thus, a measurement technique enabling correct dosing is necessary for SRT devices. The presence of microbubbles produced by SRT is a sign of RPE cell damage [12], and microbubbles can be detected by opto-acoustic (OA) and optical-feedback techniques (OFT). This function of OA has been clinically demonstrated in retinal photocoagulation [20]. A corresponding automatic control system was also successfully used in rabbits [21]. In a recent work, the use of OFT allowed us to detect microbubble-induced characteristics in the backscattered laser light quickly enough that we could cease laser irradiation within a burst, demonstrating that SRT with OFT was safe and effective [22]. Previous studies with OFT have examined only the appearance of the photoreceptors and the RPE under light microscopy. However, observation of the RPE ultrastructures is important for evaluating the efficacy of SRT. To date, no studies have evaluated the RPE and its surrounding structures using electron microscopy (EM) after SRT coupled with OFT.

Here, we evaluate the safety and selectivity of SRT treatment with OFT based on multimodal imaging assessment and systematic histologic analysis of the effects of SRT. We also describe the dynamics of healing and the reorganization of retinal lesions following therapy.

Materials and method

Animals

Six healthy Dutch Belted rabbits (12 eyes) weighing between 1.5 and 2.5 kg were bred in the laboratory animal center of the Kyung Hee University Hospital. All procedures performed in studies involving animals were in accordance with the guidelines of the Kyung Hee University Hospital Institutional Animal Care and Use and the Association For Research in Vision and Ophthalmology (ARVO) Statement for the Use of Animals in Ophthalmic and Vision Research. Rabbits were anesthetized with Zoletil 50 (125 mg zolazepam and 125 mg tiletamine hydrochloride; Virbac S.A., Carros, France; 0.2 mg/kg of body weight) and Rompun (2 % xylazine hydrochloride; Bayer Animal Health, Leverkusen, Germany; 5 mg/kg of body weight) administered intramuscularly 15 min before the procedure. The eyes were dilated with topical 0.5 % phenylephrine hydrochloride and 0.5 % tropicamide (Mydrin-P; Santen, Osaka, Japan). One drop of topical 0.5 % proparacaine hydrochloride was instilled in each eye before treatment. The experiments were conducted around the same time of day.

Changes in the retinal microstructures were assessed using fundus photography, fluorescein angiography (FAG), spectral-domain optical coherence tomography (SD-OCT), light microscopy (LM), transmission electron microscopy (TEM), and scanning electron microscopy (SEM) at the following time points: 1 h, and 1, 3, 7, 14 and 28 days after SRT.

Laser system

The SRT system used in this study was a Q-switched, frequency-doubled neodymium-doped yttrium lithium fluoride (Nd:YLF) laser-emitting light at a wavelength of 527 nm (Medical Laser Center Lübeck GmbH, Lübeck, Germany). A pulse duration of 1.7 μs was used, with a 100-Hz repetition rate. The maximum number of pulses in a single burst was limited to 30. The laser spot size diameter was 200 μm in the air. The maximum energy was set between 40 and 45 μJ. Conventional laser lesions served as visible markers to identify the location of non-visible SRT-treated lesions during histologic evaluation (Fig. 1). With regard to the visible laser lesions, a conventional continuous-wave laser system (PASCAL Streamline; Topcon Medical Laser Systems, Inc., Santa Clara, CA, USA) delivering laser irradiation at a wavelength of 532 nm was used in the left eyes of rabbits. The spot size was 400 μm in the air, the irradiation duration was 20 ms, and the laser power was 500 mW in each laser spot. Mainster central-field contact lenses with 1.05 magnification were used. Laser patterns were created in the fundus inferior to the optic nerve head. Initially, ophthalmoscopically visible marking spots were generated by continuous laser at

Fig. 1 Patterns of laser application (**a**), fundus photography (**b**), and corresponding fluorescein angiography (**c**) at 1 h after selective retina therapy (SRT) or conventional laser applications. A grid of white spots (*arrowhead*) was created by conventional laser for orientation during treatment (**b**). All SRT lesions were ophthalmoscopically invisible, while conventional laser lesions were ophthalmoscopically visible (**b**). Fluorescence angiography images showed hyperfluorescence in the areas of the damaged retinal pigment epithelium after SRT (*arrow*) (**c**)
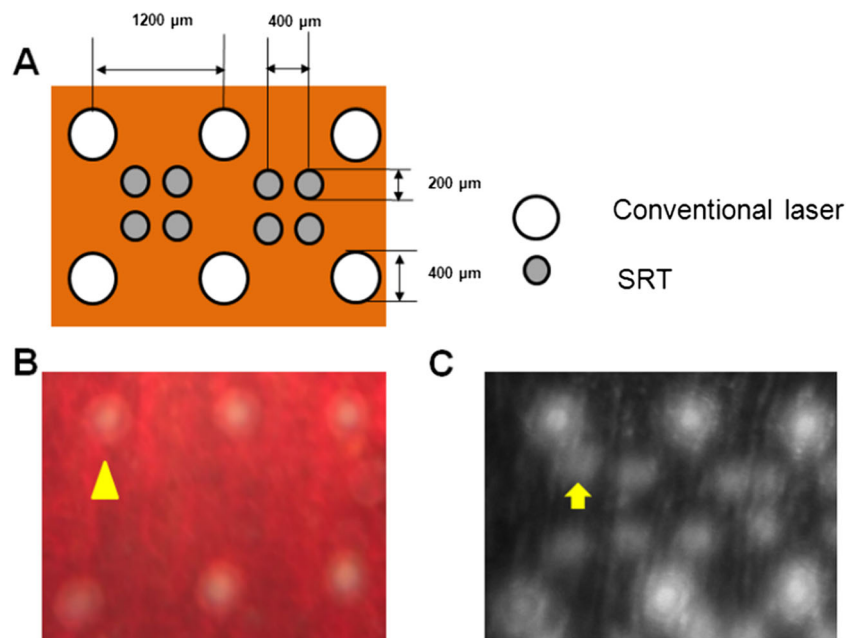
1200-μm intervals in both eyes of the Dutch Belted rabbits. Thereafter, 2 × 2 SRT laser spots were created within a rectangle of the marking spots (Fig. 1).

Because SRT lesions are usually clinically invisible during laser exposure, OFT developed and manufactured by the Medical Laser Center Lubeck was applied for dosimetry control. OFT is able to detect the ophthalmoscopically invisible laser-induced damage to the RPE, helping to overcome this practical limitation of SRT. The formation of microbubbles around the light-absorbing melanosomes inside the RPE is the hallmark of RPE damage during microsecond laser pulse exposure [12]. OFT using a photodiode detects backscattered light produced by microbubbles [22]. In automatic dosimetry control, the laser is set such that the pulse increases in a step-wise manner, and then laser irradiation automatically ceases as soon as a predefined threshold value is reached, as previously reported [22, 23].

Fundus photography and fluorescein angiography (FAG)

Fundus photographs were obtained and FAG was performed to visualize RPE defects at 1 h and 1, 3, 7, 14 and 28 days after SRT. A slow intravenous injection of 0.3 mL of fluorescein 10 % (Fluorescite; Alcon Laboratories, Hünenberg, Switzerland) was administered into the marginal ear vein, and photographs were obtained starting a few seconds after the fluorescein injection and every 15 to 20 s thereafter up to 10 min. Fundus photographs were obtained with a fundus camera (FF450^plus; Carl Zeiss Meditec, Inc., Jena, Germany), and FAG was performed using the Heidelberg Spectralis (Heidelberg Engineering, Heidelberg, Germany).

Retinal histology

Light microscopy and transmission electron microscopy

Rabbits were sacrificed at each time point by injecting an overdose of an anesthetic cocktail. Immediately after enucleation, the globes were opened circumferentially 3 mm behind the limbus. The anterior segment, lens, and remaining vitreous were removed. The posterior eyecup was placed in a 20-mL fixative solution comprising 4 % paraformaldehyde for 3 days. The area of interest on the posterior eyecup was carefully dissected and placed in fresh fixative solution. For TEM, the rabbit retina from each group was post-fixed in 1 % osmium tetroxide in phosphate-buffered saline (PBS) for 1 h. Samples were washed and dehydrated through serial dilutions of ethanol, and then mounted onto stubs, sputter-coated with gold by a Polaron SC500 (VG Microtech, Sussex, UK), and examined with TEM (JEM-1400; JEOL Ltd., Tokyo, Japan). To evaluate the histologic characteristics of the laser-treated retina, toluidine blue staining for light microscopy was performed before photographs were obtained. An ultramicrotome (Reichert-Jung Ultracut E; Leica Microsystems, Deerfield, IL, USA) was used to cut and prepare the sections for LM and TEM.

Scanning electron microscopy

For SEM, two eyes were enucleated at each time point, i.e., 1 h and 1, 3, 7, 14 and 28 days after SRT. The anterior segment, lens, and remaining vitreous and retina were removed. Samples were then pre-fixed with 4 % glutaraldehyde in PBS (pH 7.2) at 4 °C overnight. Following several washes in PBS, samples were kept in 1 % osmium tetroxide-PBS for final

fixation for 1 h. Samples were then washed and dehydrated through serial dilutions of ethanol, mounted onto stubs, sputter-coated with gold by a Polaron SC500 (VG Microtech, Sussex, UK), and examined with SEM (JSM-7401F; JEOL Ltd., Tokyo, Japan).

BrdU (5'-bromo-2'-deoxy-uridine) incorporation assay

Cell proliferation assay was performed with BrdU labeling of cross sections from SRT laser spots. Two days prior to animal sacrifice, 10 mL of BrdU (10 mg/mL in 0.9 % NaCl, pH 7.4; 100 mg/kg, Sigma-Aldrich Corp., St. Louis, MO, USA) was infused slowly into a marginal vein of rabbit ear. The enucleated eyes were embedded with OCT compound and sectioned at a thickness of 5 μm. SRT laser spots and control samples from normal retina tissue were fixed with absolute methanol (Merck, Darmstadt, Germany) for 15 min at 4 °C, followed by permeabilization with 0.3 % Triton X-100 for 5 min. Samples were treated with 1 N HCl for 1 hr at 37 °C for DNA denaturation, and then neutralized with 0.1 M borate buffer (pH 8.5) for 10 min at room temperature (RT). After washing with PBS, samples were treated with primary antibody against BrdU (1:250; Abcam plc, Cambridge, UK) in 20 % normal goat serum (NGS). Samples were washed in PBS, and then treated with anti-rat FITC secondary antibody in 20 % NGS for 1 hr at RT, and again washed in PBS. Nuclei were stained with propidium iodide (PI; Sigma-Aldrich Corp., St. Louis, MO, USA) and mounted in VECTASHIELD® mounting medium (Vector Laboratories, Cambridgeshire, UK). Images were taken under a Nuance Multiplex Biomarker Imaging System (Cambridge Research Instrumentation, Woburn, MA, USA). For quantification of cell proliferation, BrdU-positive RPE cells were manually counted using at least five cross sections for each time point. Two experienced laboratory colleagues (HSH, SMB) counted the cells in a blinded manner.

Spectral domain-optical coherence tomography

Laser-treated retinal lesions were scanned using SD-OCT (Spectralis; Heidelberg Engineering, Heidelberg, Germany) to examine changes in the anatomic structures in retinal lesions at 1 h and 1, 3, 7, 14 and 28 days, until enucleation. Dense single-raster horizontal scans and volume scans were performed on laser-treated lesions to obtain cross-sectional images of the retinal tissue. At each time point, the direct correlation between SD-OCT and histology was assessed for interpretation of the various retinal layers.

Statistical analysis

We used Mann–Whitney and Kruskal–Wallis tests to compare the total number of BrdU-positive RPE cells at each time point. Statistical analysis was conducted using SPSS software version 18.0 for Windows (SPSS, Inc., Chicago, IL, USA), and $P < 0.05$ was considered statistically significant.

Results

Fundus photography and FAG

SRT lesions

On fundus photographs, only those marking spots created with the conventional laser were visible and SRT lesions were invisible at 1 h after SRT. FAG detected hyperfluorescence corresponding to the SRT laser spots (Fig. 1). On day 1 following SRT, fundus photographs showed mild pigmentation on the SRT lesion, and FAG detected hyperfluorescence of all SRT lesions (Fig. 2). Fundus photographs showed further pigmentation on day 3. Hyperfluorescence of SRT lesions decreased on day 3 and was barely noticeable by day 7.
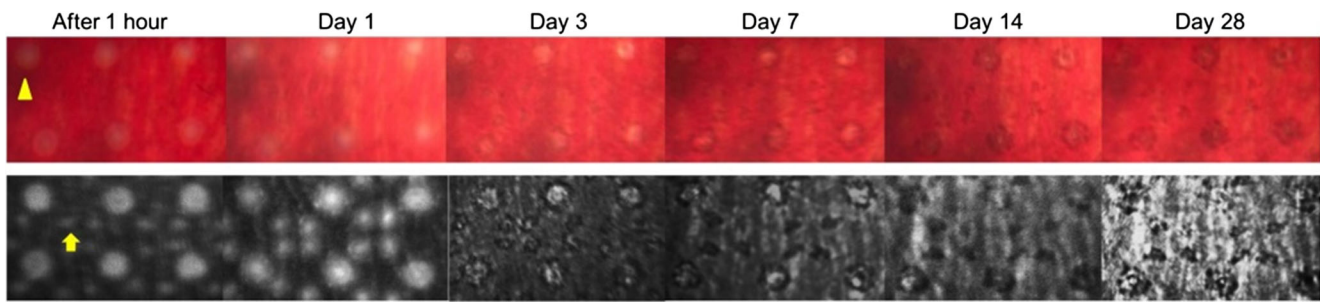
Conventional laser lesions

Conventional laser lesions were visible on fundus photographs after laser treatment. FAG detected hyperfluorescence on the spots where conventional laser irradiation had been applied (Fig. 1). Hyperfluorescence caused by a window defect was still observed on day 7 after laser irradiation. Hyperpigmented lesions were detected on fundus photographs and hyperfluorescence decreased after 14 days (Fig. 2). In FAG, hypofluorescence was evident on day 28.

LM and SD-OCT

SRT lesions

Light microscopy(LM) showed RPE layer collapse following SRT, i.e., irregularities in the RPE layer with a focal space between RPE and photoreceptors at 1 h after laser irradiation (Fig. 3a-1). Regular neurosensory structures were observed after 1 h on SD-OCT (Fig. 3b-1). On LM, there was no difference between 1 h and 1 day after SRT. On day 1, SD-OCT images of SRT lesions revealed mild thinning of the RPE layer and decreased reflectivity (Fig. 3b-2). The overlying retina remained intact. On day 3, LM showed decreased space between the RPE and photoreceptor layer (Fig. 3a-3). On day 7, RPE thickening was observed on LM (Fig. 3a-4), and there was a corresponding increase in the reflectivity of the lesions on SD-OCT (Fig. 3b-4). The fluid-filled space became smaller. On days 14 and 28, LM revealed normal-appearing photoreceptors and RPE with mild hypertrophy (Fig. 3a-5, a-6). Correspondingly, SRT lesions were restored to normal

Fig. 2 Consecutive changes shown in a series of fundus photographs and fluorescein angiography (FAG) findings after selective retina therapy (SRT) and conventional laser treatment. On fundus photography, SRT lesions were ophthalmoscopically invisible at first and then showed increasing pigmentation after 3 days. In conventional laser treatment, whitish lesions were observed immediately after laser irradiation (*arrowhead*). Hyperpigmentation was observed after 7 days. On FAG, hyperfluorescence was observed immediately after laser irradiation on SRT lesions (*arrow*). Hyperfluorescence began to decrease after 3 days and disappeared after 7 days. In conventional laser treatment, hyperfluorescence lasted 14 days and then disappeared by day 28

morphologic structures on SD-OCT from 14 through 28 days (Fig. 3b-5, b-6).

Conventional laser lesions

OCT and LM images generated by lesions irradiated with conventional laser differed from those of SRT lesions. On LM, full-thickness damage was evident in conventional laser-treated lesions 1 h after laser

irradiation (Fig. 3c-1). SD-OCT findings after conventional laser showed irreversible changes consistent with those observed on LM images. SD-OCT showed increased reflectivity throughout the full thickness of the neurosensory layer and the retinal structure, and delineation of the individual layers within the retina was absent, corresponding to the histologic findings 1 h after laser irradiation (Fig. 3d-1). White columns were visible throughout all retinal layers.
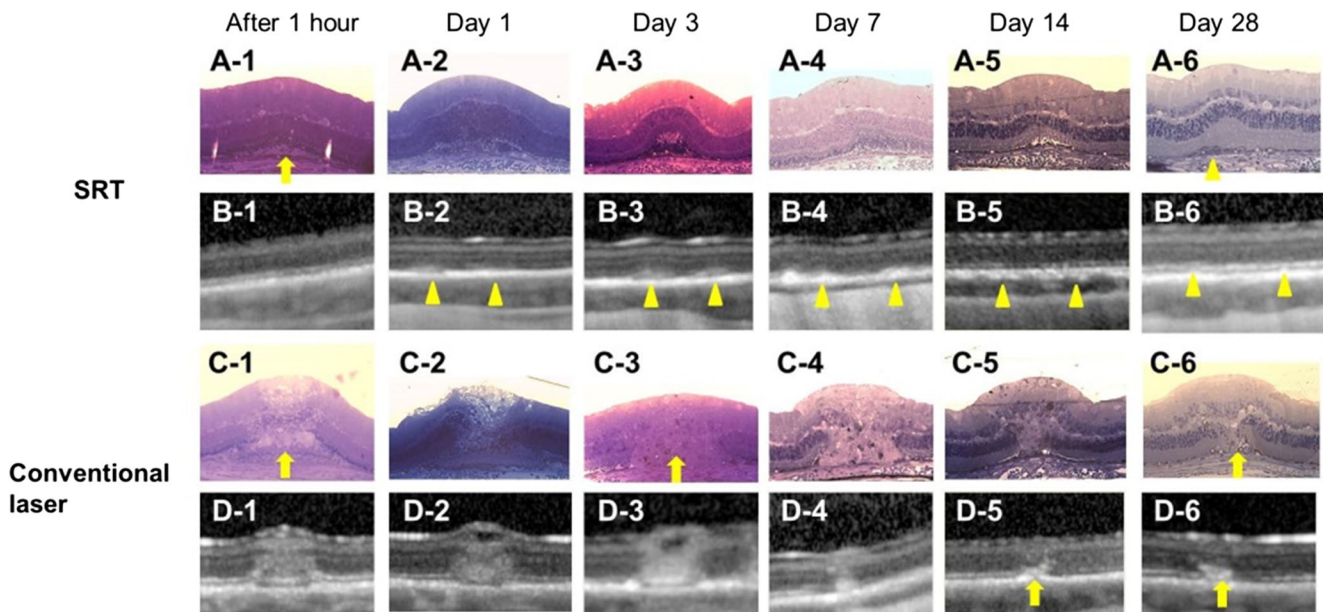
Fig. 3 Histologic appearance and spectral domain optical coherence tomography (SD-OCT) images obtained at each time point after selective retina therapy (SRT) and conventional laser. On light microscopy (LM), the retinal pigment epithelium (RPE) layer following SRT exhibited increasing irregularity, with focal fluid collected between the RPE and photoreceptor layer at 1 h (*arrow*) (a-1). Fluid was absorbed over time. On day 28, LM showed a normal-appearing RPE, with mild hypertrophy (*arrowhead*) (a-6). LM after conventional laser, however, showed irreversible changes. The zone of damage clearly extended from the RPE throughout the retina, including the photoreceptors (*arrow*) (c-1). The neurosensory retina was replaced by fibrous tissue (*arrow*) (c-3). On day 28, the damage to the photoreceptors was not completely restored, and the RPE had an irregular contour (*arrow*) (c-6). SD-OCT images obtained 1 h after SRT showed the unaffected neurosensory retina on the SRT lesions (B-1), whereas severe damage to the neurosensory retina irradiated with conventional laser was seen (d-1). On day 1, SRT lesions showed mild thinning of the RPE layer and a decline in reflectivity (*arrowhead*) (b-2). RPE thickening coupled with increased reflectivity was observed on day 3 (*arrowhead*) (b-3). Areas of SRT lesions were restored to normal morphologic structures from 14 to 28 days (b-6). Destruction of the RPE and inner segment/outer segment layer was observed, however, on day 3 in conventional laser (*arrow*) (c-3). On days 14 and 28, generalized atrophic changes were observed on lesions treated with conventional laser (*arrow*) (d-5, d-6)

On day 3, LM showed gliosis on the lesion treated with the conventional laser, which presented as increased reflectivity in bands on OCT (Fig. 3c-3, d-3). Although the retinal edema was markedly decreased, destruction of the RPE and inner segment/outer segment (IS/OS) layer persisted on SD-OCT.

On day 7, LM showed a thicker RPE (Fig. 3c-4), and focal hyperreflectivity was observed in the RPE and photoreceptor layer on SD-OCT (Fig. 3d-4). On day 14, LM showed restoration of the RPE layer and mild hypertrophy of RPE cells, but the photoreceptors were not completely restored (Fig. 3c-5). On day 28, LM showed a glial plug present in the center of the irradiated lesion with no photoreceptor cells (Fig. 3c-6). On days 14 and 28, SD-OCT images revealed highly reflective signals on the RPE and photoreceptor layer and contraction of the neurosensory layers, suggesting tissue scarring (Fig. 3d-5, d-6).

SEM and TEM

SRT lesions

One hour after treatment, SEM of the RPE showed limited damage in the center of the SRT burn, and the surrounding cells seemed to have normal morphology (Fig. 4a). TEM showed vacuolization in the cytoplasm of the RPE (Fig. 5a). Disrupted outer segments of photoreceptors were observed. Fluid had accumulated between the RPE and the photoreceptors due to RPE destruction. The RPE was flattened, and some of the RPE cytoplasm was swollen. On day 3, SEM showed

migration of the surrounding RPE cells to restore continuity in the damaged area (Fig. 4b). TEM disclosed a lack of organelles and decreased melanin granule density in the cytoplasm. RPE cells were swollen, and the outer segments of the photoreceptors were damaged (Fig. 5b).

SEM on day 7 demonstrated recovery of the RPE monolayer in the center of the irradiated lesion, which comprised RPE cells of various sizes (Fig. 4c). Some RPE cells formed double or multilayers. Microvilli on the apical surface, however, were limited and not completely restored in the SRT lesion (Fig. 4f). TEM revealed flattened and polygonal RPE cells (Fig. 5c). The decreased cytoplasmic density was restored to a normal level and the density of melanin granules increased. Microvilli on the apical surface and interdigitation with photoreceptors were not observed.

On days 14 and 28, recovery of the RPE layer of the SRT lesion was observed on SEM (Fig. 4d, e). The microvilli on the RPE apical surface were completely restored on day 28 (Fig. 4g). On TEM, polygonal RPE cells were observed, and some RPE cells migrated to other RPE cells to form a bilayer on day 14 (Fig. 5d). In the cytoplasm, normal cytoplasmic organelles such as the Golgi complex and tight junctions were observed, and the density of melanin granules was decreased from the previously measured level (Fig. 5f). Interdigitation between the RPE and photoreceptor layer was partially observed. The outer segments of photoreceptors appeared normal. On day 28, the microvilli on the apical surface and the normal apical-basal polarity were observed (Fig. 5g). Many phagosomes were present in the cytoplasm.
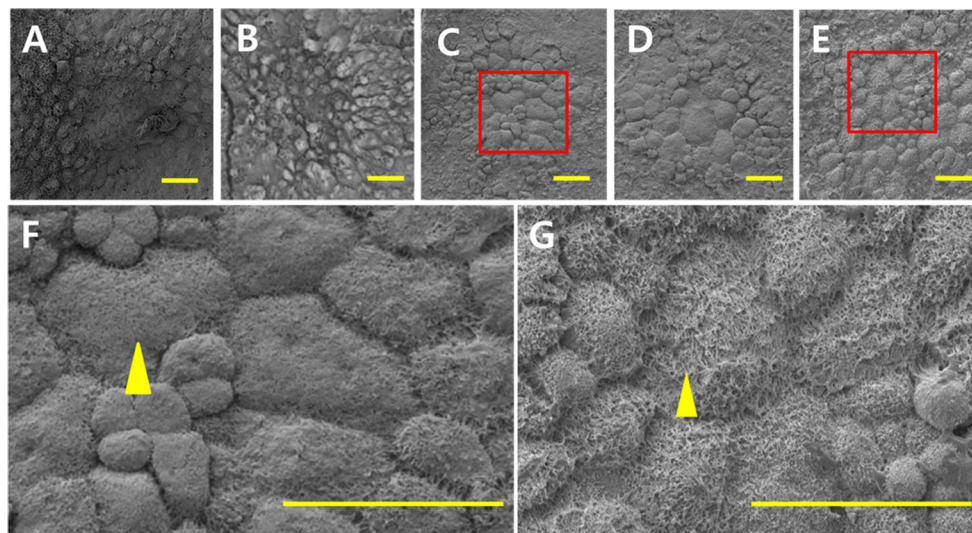
Fig. 4 Consecutive changes shown on scanning electron microscopy (SEM) after selective retina therapy (SRT). At 1 h, focal retinal pigment epithelium (RPE) damage was evident in the center of the SRT lesion (a). On day 3, RPE cells from the periphery of the wound began to migrate into the damaged zone (b). On day 7, SEM demonstrated restoration of the RPE layer consisting of small and large RPE cells in the center of the lesion created by SRT (c). Some double- or multilayered RPE was also observed. On days 14 and 28, the RPE layer was more densely packed with RPE cells of different sizes (d, e). A magnified view of the area within the *red square* in (c); RPE monolayer cells in the center of the region of laser exposure on day 14 (f). Microvilli on the apical surface were limited (*arrowhead*). A magnified view of the area within the *red square* in (e); RPE layer cells on day 28 (g). Microvilli on the RPE apical surface were completely restored (*arrowhead*). *Scale bar* = 50 μm
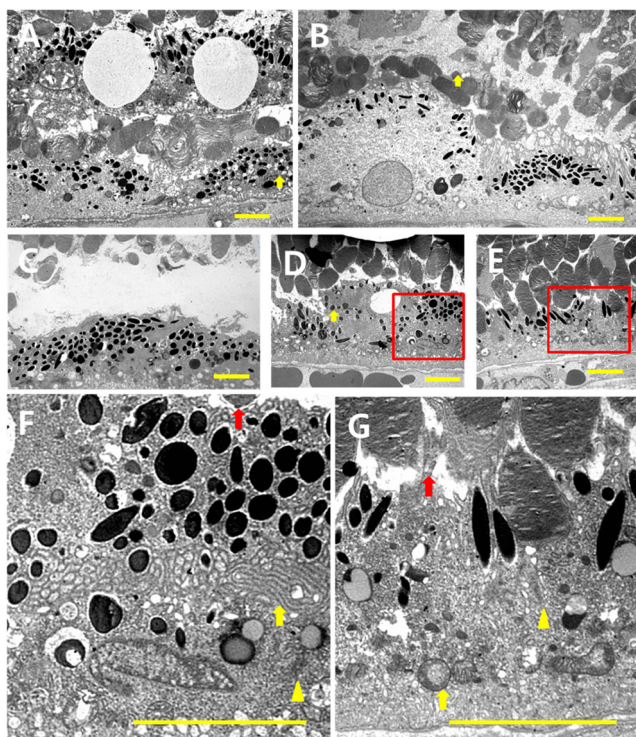
Fig. 5 Images generated by transmission electron microscopy (TEM) after selective retina therapy (SRT). At 1 h, microvesicles were observed in the cytoplasm (*arrow*) (**a**). At day 3, TEM demonstrated a lack of organelles and decreased density of melanin granules in the cytoplasm (**b**). Some of the retinal pigment epithelium (RPE) cytoplasm was swollen. Damage to the outer segment of the photoreceptors was observed (*arrow*). At 7 days, flattened RPE cells were evident, and cytoplasm density returned to normal. The density of melanin granules increased. There was no evidence of microvilli on the apical surface or interdigitation between photoreceptors and RPE (**c**). At 14 days, polygonal RPE cells were observed, and some RPE cells migrated to other RPE cells to form a bilayer (*arrow*). The density of melanin granules decreased (**d**). At 28 days, normal apical-basal polarity was observed (**e**). A magnified view of the area within the red square in (**d**) on day 14 (**f**). Microvilli on the apical surface were limited (*red arrow*). A Golgi complex was observed in the cytoplasm (*arrow*), and a tight junction was evident (*arrowhead*). A magnified view of the area within the *red square* in (**e**) on day 28 (**g**). Microvilli on the apical surface (*red arrow*) and many phagosomes were observed in the cytoplasm (*arrow*). A tight junction was also observed (*arrowhead*). *Scale bar* = 5 μm

Conventional laser lesions

On SEM, destruction of the RPE was evident in lesions treated with conventional laser at 1 h after treatment (Fig. 6a). TEM showed vacuolization in the cytoplasm of RPE cells and diffuse disruption of photoreceptors (Fig. 7a).

On day 3, RPE destruction was still evident on SEM (Fig. 6b). On TEM, an absence of intracellular organelles was observed, except for pigment granules in the RPE cytoplasm. There was a diffuse disorganization of the photoreceptors (Fig. 7b).

SEM on day 7 showed limited RPE restoration, with an irregular-shaped RPE layer (Fig. 6c). No distinct microvilli were observed on the apical surface of RPE cells (Fig. 6f).

TEM disclosed enlarged, flattened polygonal RPE cells. The density of melanin granules was increased in the cytoplasm. Microvilli on the apical surface and interdigitation with photoreceptors were not evident (Fig. 7c).

On day 14, SEM demonstrated recovery of the RPE monolayer comprising RPE cells of various sizes (Fig. 6d). On TEM, some RPE cells forming multilayers seemed to have unusually large amounts of cytoplasm and a high density of melanin granules (Fig. 7d). There were no visible tight junctions in the cytoplasm. These RPE cells lost their apical-basal polarity. Microvilli on the apical surface were limited. SEM on day 28 showed restoration of the RPE monolayer comprising RPE cells of various sizes (Fig. 6e), and microvilli were present on the apical surface of RPE cells (Fig. 6g). On TEM, restored RPE cells formed multilayers mixed with photoreceptor cells (Fig. 7e). These RPE cells lacked apical-basal polarity in the cytoskeletal organization of the melanin granules and mitochondria. Interdigitation between the RPE and photoreceptors was observed.

BrdU incorporation assay

Cell proliferation was confirmed by BrdU labeling on day 3, with fewer BrdU-positive RPE cells in the SRT lesions (Fig. 8a) than on day 7 (Fig. 8b). On day 7, cross-sectional images demonstrated a burst of BrdU-positive RPE cells which are considered as increased potential cell proliferation activity. However, on day 14, the total number of BrdU-positive RPE cells markedly decreased (Fig. 8c), whereas no RPE proliferation was observed on day 28 (Fig. 8d). The mean (±SD, standard deviation) number of BrdU-positive RPE cells was 3.2 ± 1.2 on day 3, 8.8 ± 2.6 on day 7, 1.4 ± 1.1 on day 14, and no positive cells on day 28 which showed significant difference between each point of time ($P = 0.004$). Along with the burst of cell proliferation observed on day 7, the difference between day 3 and 7 was also significant ($P = 0.008$).

Discussion

RPE dysfunction is found in several macular diseases, including drusen, diabetic macular edema, and central serous chorioretinopathy, suggesting the need to specifically target the RPE with macular therapy in these conditions. SRT is performed by applying laser pulses with pulse durations shorter than the thermal relaxation time needed for the produced heat to diffuse [12]. Thermomechanical disruption of the RPE occurs because of microbubbles formed following vaporization around intracellular melanosomes after pulse durations of less than 10 μs [12]. The pigmentation variation in the RPE and invisibility of SRT lesions, however, make it
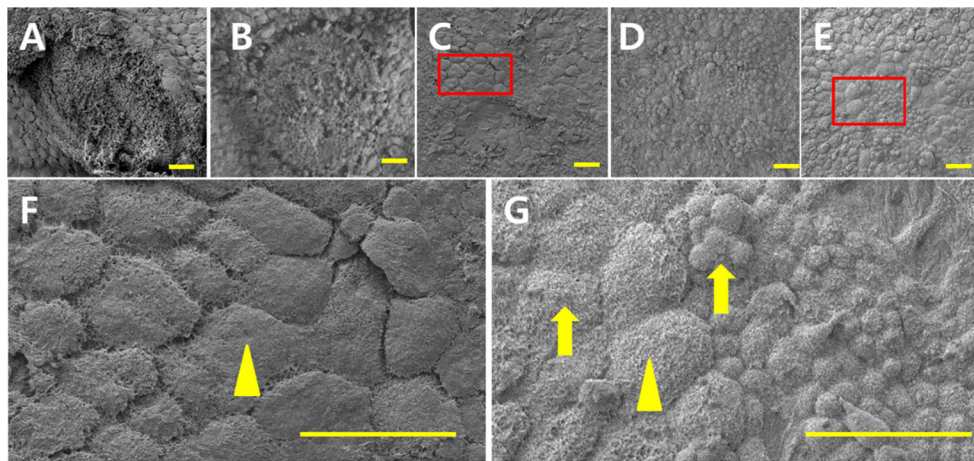
Fig. 6 Consecutive changes in the lesion in a series of images obtained by scanning electron microscopy (SEM) after conventional laser treatment. SEM at 1 h showed destruction of the retinal pigment epithelium (RPE) in the conventional laser lesion, while surrounding cells seemed to remain intact (**a**). On day 3, diffuse RPE destruction was apparent (**b**). On day 7, SEM showed limited RPE restoration, with an irregular-shaped RPE layer (**c**). On day 14, it was clear that the restored RPE layer comprised RPE cells of different sizes (**d**). On day 28, recovery of the RPE layer was observed (**e**). A magnified view of the area within the *red square* in C (**f**). Apical surface of the RPE appeared smooth, with no clearly visible microvilli (*arrowhead*). A magnified view of the area within the *red square* in (**d**) (**g**). Microvilli on the apical surface of the RPE were observed (*arrowhead*). The RPE layer comprised RPE cells of various sizes (*arrow*). *Scale bar* = 5 μm

difficult to determine the proper titration of the treatment [19, 23], and thus an automatic irradiation control system is needed. An optical feedback technique (OFT) is an automatic control system that is able to detect backscattered light generated by microbubbles and stop laser irradiation when a certain threshold is reached [22]. Recently published papers have demonstrated the high selectivity and safety of SRT coupled with OFT [22, 23]. These studies used LM for histologic
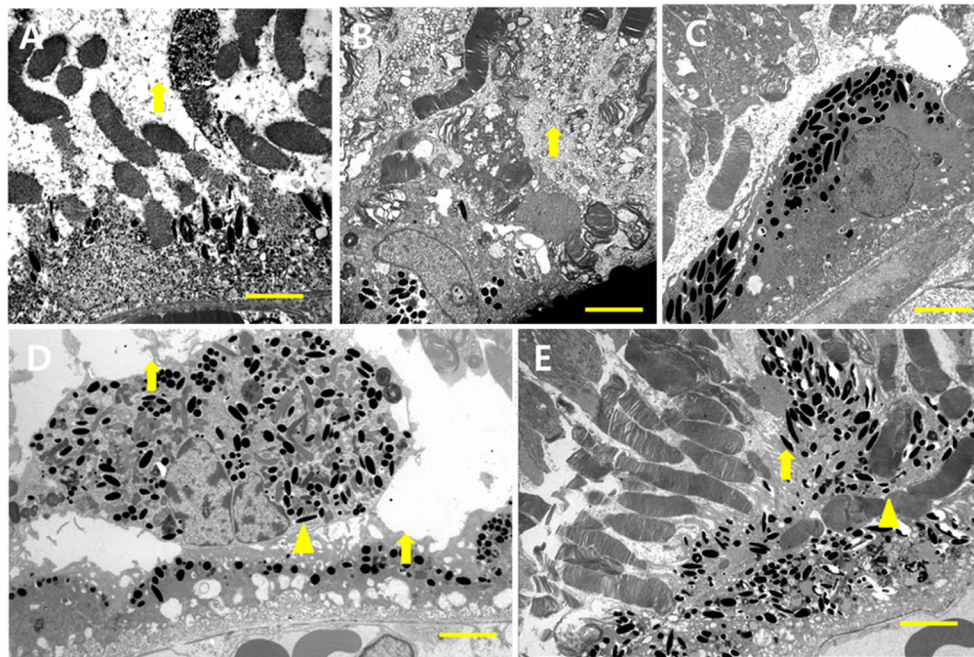
Fig. 7 Images obtained by transmission electron microscopy (TEM) after conventional laser treatment. On day 1, TEM showed an absence of intracellular organelles except for pigment granules in the retinal pigment epithelium (RPE) cytoplasm, with diffuse destruction of photoreceptors (*arrow*) (**a**). On day 3, TEM showed extensive destruction of photoreceptors (*arrow*) (**b**). On day 7, enlarged RPE cells were apparent, and increased density of melanin granules was observed. Microvilli on the apical surface were not evident (**c**). On day 14, few microvilli were observed on the apical surface (*arrow*). Some RPE cells making up the multilayer and cytoplasm were observed in an unusually large and high density of melanin granules, coupled with a loss of apical basal polarity (*arrowhead*) (**d**). On day 28, TEM demonstrated that the RPE cells replacing the old cells formed a multilayer mixed with photoreceptor cells (*arrowhead*). These RPE lacked apical-basal polarity, with an increased density of melanin granules. Interdigitation between the RPE and photoreceptors was observed (*arrow*) (**e**). *Scale bar* = 5 μm
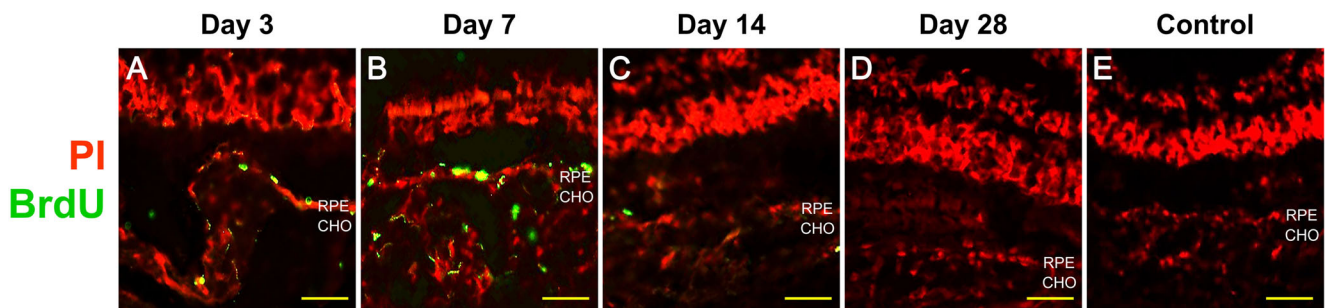
Fig. 8 Representative images of cross sections of the retina with BrdU (5'-bromo-2'-deoxy-uridine, green) and PI (PIpropidium iodide, red) immunostaining after selective retina therapy. Merged images represent BrdU-positive retinal pigment epithelium (RPE) cells on day 3 (**a**), with peak proliferation observed on day 7 (**b**), followed by markedly reduced BrdU labeling until days 14 and 28 (**c**, **d**). Only a few BrdU-positive RPE cells were observed on day 14 (**c**), and no BrdU labeling was observed on day 28 (**d**). BrdU immunostaining of non-lasered retina from the same rabbit at day 3 shows no signs of BrdU uptake (**e**). *Scale bar* = 100 μm

assessment and ERG for functional analysis. In SRT with OFT, however, it is important to ensure dynamic healing not only of the photoreceptors and the RPE but of its ultrastructures as well, including tight junctions, melanosomes, and microvilli. Therefore, we used LM, SEM, TEM, and multimodal imaging to evaluate the morphologic changes in the RPE and its surrounding structures in response to SRT with OFT.

On FAG, hyperfluorescence was observed immediately after SRT, and began to decrease on day 3, with hypofluorescence observed on day 7. This progression matches that observed in fundus examination of focal retinal hyperpigmentation. Lopez et al. reported that focal retinal hyperpigmentation was correlated with RPE hyperplasia [24], and RPE hyperplasia may occur during the healing process following SRT, leading to hyperpigmentation represented by hypofluorescence in FAG. In other words, the resolution of hyperfluorescence at 1 week corresponds to the anatomic finding of the restoration of RPE continuity at 1 week. With conventional laser therapy, however, hypofluorescence was first observed on day 14, which indicates that more time was needed for fully recovery of the RPE layer due to the extensive damage to the RPE and its surrounding tissues.

We observed serial changes in vivo using SD-OCT following laser irradiation. At 1 h after SRT, no significant change was observed on SD-OCT, but a focal fluid collection was detected between the RPE and photoreceptors on LM. LM showed that the RPE on the SRT lesions recovered over time, with no serious damage to the photoreceptors. We also confirmed on OCT that the RPE grew thicker and the RPE band had higher reflectivity, while the IS/OS layer remained intact. On the other hand, the whole retinal layer irradiated with conventional laser was destroyed based on LM, and a full thickness increase in the reflectivity was observed within the neurosensory retina on SD-OCT. Such lesions became localized over time. Glial tissues were observed on LM, however, and hyperreflective signals were present on SD-OCT, even after 28 days, around the spot corresponding to the glial plug.

Recent papers reported that the SD-OCT findings correlated with histology in animal models after laser photocoagulation [25]. In our study, OCT findings were also well correlated with LM findings, consistent with previous results. These findings demonstrated that well-known histologic characteristics could be monitored in vivo on SD-OCT after laser treatment.

With regard to outcomes based on EM, at 1 h and 1 day after SRT, only Bruch's membrane was visible. The RPE layer began to recover on day 7, when the RPE monolayer was discernible on SEM and TEM. TEM also indicated recovery of the cytoplasm starting on day 7. RPE multilayers began to form on day 14 and were clearly visible on day 28. It was not clear whether restoration of the RPE originated from the native RPE or hyperplastic RPE. Lavinsky et al. noted that native RPE migration took place on day 3, followed by RPE proliferation on day 7 [12]. Oganesian et al. [26] reported that RPE proliferation resulted from sliding of hyperplastic descendants of native RPE cells. Although the study failed to show any mitotic features of RPE cells, the authors cited sampling error as a possibility due to the very short RPE mitotic cycle [24, 26]. We found that RPE monolayers were formed first in the initial stage, followed by multilayer formation, and then small cells with prominent microvilli were visible in the multilayered RPE, as reported by Lavinsky [27]. Moreover, BrdU incorporation assay from our results revealed prominent RPE proliferation on day 7, after the identification of proliferation on day 3. These findings led us to conclude that the RPE sliding migration occurred first, followed by RPE proliferation.

Tight junctions are typically re-established among multilayered RPE cells by day 14. Lavinsky et al., however, reported the restoration of tight junctions after 3 days [27]. In our study, FAG showed very clear hypofluorescence on day 7, and LM revealed a reduction in the fluid between the RPE and photoreceptors on day 7, indicating that the tight junctions could have occurred before day 14. A sampling error may have prevented them from making this observation within

7 days. These findings suggest that re-formation of the RPE tight junctions provides an ultrastructural basis upon which the outer blood–retinal barrier is restored during RPE wound healing [26].

Recent papers have reported the restoration of normal photoreceptor structure over time due to migration after SRT [13, 28]. In our study, photoreceptors were not completely damaged so it is difficult to observe the restoration to the migration. The outer segments of the photoreceptors, which were shortened and disorganized following SRT, were restored within 2 weeks after SRT. All of the anatomic changes were resolved and the normal structure was restored within weeks after SRT. These findings indicate that the photoreceptor function remains intact as the inner segments of photoreceptors and outer nuclear layer all remain intact following SRT.

We found that where the photoreceptors remained intact to some extent, the SRT lesions were quickly restored, while the recovery took longer in the conventional laser lesions where photoreceptors were severely damaged. These results suggest that photoreceptor–RPE trophic factor interactions or restored interdigitation between the RPE and photoreceptors are responsible for the reacquisition of normal photoreceptors and RPE cells [29–31].

Our study used FAG in order to evaluate RPE damage. In contrast, Framme's studies used non-invasive autofluorescence imaging to confirm a reduction in autofluorescence (online measurements) as an indication of damage to the RPE immediately after SRT [32, 33], and also reported hyper-autofluorescence at 1 week [33]. The anatomic outcome in our study and the autofluorescence findings in Frammes's study [33] suggest that hypo-autofluorescence observed at day 1 after SRT was due to destruction of the RPE, and the RPE proliferation observed at week 1 led to hyper-autofluorescence. Further autofluorescence studies following SRT are sure to produce meaningful results for important applications in the clinical setting.

A comparison of conventional laser and SRT in this study using EM indicated that ultrastructures of the RPE recovered quickly after SRT. Results also confirmed that conventional laser therapy resulted in damage not only to the RPE and photoreceptors, but also the inner retina, whereas in SRT, the tight junctions, microvilli, and interdigitation between the RPE and photoreceptor layer were all restored, despite some damage to the RPE and outer segments of the photoreceptors. In addition, the disadvantages of existing subthreshold laser or under-treating titration were resolved by SRT with OFT, as treatment effects can be confirmed with histologic examination and OCT.

In addition, SRT appears to effectively treat macular disease by inducing the formation of new ultrastructures in the RPE, which include tight junctions, microvilli, apical-basal polarity, and interdigitation between the RPE and photoreceptors. Another mechanism underlying SRT efficacy is the activation of a cellular cascade. Changes in the RPE are induced by the stimulation of factors released as a result of laser injury. Platelet-derived growth factor, vascular endothelial growth factor, and pigment epithelium-derived factor, for example, are released from surviving RPE cells that have been directly or indirectly physically or chemically stressed [34–37].

The limitations of this study include optical handicaps due to various conditions including corneal edema and media opacity. Restoration of the RPE was not evaluated using an immune assay or other means, which would have helped reveal a clear mechanism. In addition, various cytokines were not evaluated after SRT.

In conclusion, selective targeting of the RPE using SRT with OFT is a promising new modality for treating macular disease. This new approach is characterized by enhanced selectivity and lack of permanent damage to the neural retina. In addition, it does not require manual adjustment by the operator based on the amount of pigment in retina, as the system operates by automatically adjusting the laser power with OFT. These features make SRT laser a particularly desirable therapy for diseases of the retina, and macular disease in particular.

Conflict of interest   All authors involved in this study certify that they have no affiliations with or involvement in any organization or entity with any financial interest (such as honoraria; educational grants; participation in speakers' bureaus; membership, employment, consultancies, stock ownership, or other equity interest; or expert testimony or patent-licensing arrangements) or non-financial interest (such as personal or professional relationships, affiliations, knowledge or beliefs) in the subject matter or materials discussed in this manuscript.

References

1. Early Treatment Diabetic Retinopathy Study Research Group (1987) Treatment techniques and clinical guidelines for photocoagulation of diabetic macular edema. Early treatment diabetic retinopathy study report number 2. Ophthalmology 94:761–74

2. Gabel VP, Birngruber R, Hillenkamp F (1978) Visible and near infrared light absorption in pigment epithelium and choroid. In: Shimizu K (ed) International congress series No. 450, XXIII concilium ophthalmologicum, Kyoto. Excerpta Medicapp, Princeton, pp 658–62

3. Birngruber R, Hillenkamp F, Gabel VP (1985) Theoretical investigations of laser thermal retinal injury. Health Phys 48:781–796

4. Lorenz B, Birngruber R, Vogel A (1989) Quantifizierung der Wellenlängenabhängigkeitlaser induzierter Aderhauteffekte. Fortschr Ophthalmol 86:644–654

5. Marshall J, Mellerio J (1968) Pathological development of retinal laser photocoagulations. Exp Eye Res 7:225–230

6. Schatz H, Madeira D, McDonald HR, Johnson RN (1991) Progressive enlargement of laser scars following grid laser photocoagulation for diffuse diabetic macular edema. Arch Ophthalmol 109:1549–1551

7. Wallow IH, Birngruber R, Gabel VP, Hillenkamp F, Lund OE (1975) Netzhautreaktionnach Intensivlichtbestrahlung. Adv Ophthalmol 31:159–232

8. Pearson AR, Tanner V, Keightley SJ, Casswell AG (1998) What effect does laser photocoagulation have on driving visual fields in diabetics. Eye (Lond) 12:64–8

9. Ulbig MR, Arden GB, Hamilton AM (1994) Color contrast sensitivity and pattern electroretinographic findings after diode and argon laser photocoagulation in diabetic retinopathy. Am J Ophthalmol 117:583–8

10. Roider J, Hillenkamp F, Flotte T, Birngruber R (1993) Microphotocoagulation: selective effects of repetitive short laser pulses. Proc Natl Acad Sci U S A 90:8643–7

11. Bresnick GH (1983) Diabetic maculopathy: a critical review highlighting diffuse macular edema. Ophthalmology 90:1301–17

12. Brinkmann R, Roider J, Birngruber R (2006) Selective retina therapy (SRT): a review on methods, techniques, preclinical and first clinical results. Bull Soc Belge Ophtalmol 302:51–69

13. Elsner H, Pörksen E, Klatt C, Bunse A, Theisen-Kunde D, Brinkmann R, Birngruber R, Laqua H, Roider J (2006) Selective retina therapy in patients with central serous chorioretinopathy. Graefes Arch Clin Exp Ophthalmol 244:1638–45

14. Roider J, Michaud NA, Flotte TJ, Birngruber R (1992) Response of the retinal pigment epithelium to selective photocoagulation. Arch Ophthalmol 110:1786–92

15. Laursen ML, Moeller F, Sander B, Sjoelie AK (2004) Subthreshold micropulse diode laser treatment in diabetic macular oedema. Br J Ophthalmol 88:1173–9

16. Parodi MB, Spasse S, Iacono P, Di Stefano G, Canziani T, Ravalico G (2006) Subthreshold grid laser treatment of macular edema secondary to branch retinal vein occlusion with micropulse infrared (810 nanometer) diode laser. Ophthalmology 113:2237–42

17. Roider J, Brinkmann R, Wirbelauer C, Laqua H, Birngruber R (2000) Subthreshold (retinal pigment epithelium) photocoagulation in macular diseases: a pilot study. Br J Ophthalmol 84:40–7

18. Yu AK, Merrill KD, Truong SN, Forward KM, Morse LS, Telander DG (2013) The comparative histologic effects of subthreshold 532- and 810-nm diode micropulse laser on the retina. Invest Ophthalmol Vis Sci 54:2216–24

19. Schmidt SY, Peisch RD (1986) Melanin concentration in normal human retinal pigment epithelium. Regional variation and age-related reduction. Invest Ophthalmol Vis Sci 27:1063–7

20. Brinkmann R, Koinzer S, Schlott K, Ptaszynski L, Bever M, Baade A, Luft S, Miura Y, Roider J, Birngruber R (2012) Real-time temperature determination during retinal photocoagulation on patients. J Biomed Opt 17:061219

21. Schlott K, Koinzer S, Ptaszynski L, Bever M, Baade A, Roider J, Birngruber R, Brinkmann R (2012) Automatic temperature controlled retinal photocoagulation. J Biomed Opt 17:061223

22. Park YG, Seifert E, Roh YJ, Theisen-Kunde D, Kang S, Brinkmann R (2014) Tissue response of selective retina therapy by means of a feedback-controlled energy ramping mode. Clin Experiment Ophthalmol 42:846–55

23. Kim HD, Han JW, Ohn YH, Brinkmann R, Park TK (2014) Functional evaluation using multifocal electroretinogram after selective retina therapy with a microsecond-pulsed laser. Invest Ophthalmol Vis Sci 56:122–31

24. Lopez PF, Yan Q, Kohen L, Rao NA, Spee C, Black J, Oganesian A (1995) Retinal pigment epithelial wound healing in vivo. Arch Ophthalmol 113:1437–46

25. Lavinsky D, Cardillo JA, Mandel Y, Huie P, Melo LA, Farah ME, Belfort R, Palanker D (2013) Restoration of retinal morphology and residual scarring after photocoagulation. Acta Ophthalmol 91:315–23

26. Oganesian A, Bueno E, Yan Q, Spee C, Black J, Rao NA, Lopez PF (1997) Scanning and transmission electron microscopic findings during RPE wound healing in vivo. Int Ophthalmol 21:165–75

27. Lavinsky D, Chalberg TW, Mandel Y, Huie P, Dalal R, Marmor M, Palanker D (2013) Modulation of transgene expression in retinal gene therapy by selective laser treatment. Invest Ophthalmol Vis Sci 54:1873–80

28. Paulus YM, Jain A, Gariano RF, Stanzel BV, Marmor M, Blumenkranz MS, Palanker D (2008) Healing of retinal photocoagulation lesions. Invest Ophthalmol Vis Sci 49:5540–5

29. Elner SG, Elner VM (1996) The integrin superfamily and the eye. Invest Ophthalmol Vis Sci 37:696–701

30. Rizzolo LJ (1991) Basement membrane stimulates the polarized distribution of integrins but not the Na, K-ATPase in the retinal pigment epithelium. Cell Regul 2:939–49

31. Rodriguez-Boulan E, Nelson WJ (1989) Morphogenesis of the polarized epithelial cell phenotype. Science 245:718–25

32. Prahs P, Walter A, Regler R, Theisen-Kunde D, Birngruber R, Brinkmann R, Framme C (2010) Selective retina therapy (SRT) in patients with geographic atrophy due to age-related macular degeneration. Graefes Arch Clin Exp Ophthalmol 248:651–8

33. Framme C, Brinkmann R, Birngruber R, Roider J (2002) Autofluorescence imaging after selective RPE laser treatment in macular diseases and clinical outcome: a pilot study. Br J Ophthalmol 86:1099–106

34. Li R, Maminishkis A, Wang FE, Miller SS (2007) PDGF-C and D induced proliferation/migration of human RPE is abolished by inflammatory cytokines. Invest Ophthalmol Vis Sci 48:5722–32

35. Pons M, Marin-Castaño ME (2011) Nicotine increases the VEGF/PEDF ratio in retinal pigment epithelium: a possible mechanism for CNV in passive smokers with AMD. Invest Ophthalmol Vis Sci 52:3842–53

36. Sonoda S, Sreekumar PG, Kase S, Spee C, Ryan SJ, Kannan R, Hinton DR (2009) Attainment of polarity promotes growth factor secretion by retinal pigment epithelial cells: relevance to age-related macular degeneration. Aging (Albany NY) 2:28–42

37. Zhu J, Wang YS, Zhang J, Zhao W, Yang XM, Li X, Jiang TS, Yao LB (2009) Focal adhesion kinase signaling pathway participates in the formation of choroidal neovascularization and regulates the proliferation and migration of choroidal microvascular endothelial cells by acting through HIF-1 and VEGF expression in RPE cells. Exp Eye Res 88:910–8